High optical quality polycrystalline indium phosphide grown on metal substrates by metalorganic chemical vapor deposition

Maxwell Zheng,[1,2] Zhibin Yu,[1,2] Tae Joon Seok,[1] Yu-Ze Chen,[3] Rehan Kapadia,[1,2] Kuniharu Takei,[1,2] Shaul Aloni,[4] Joel W. Ager,[2] Ming Wu,[1] Yu-Lun Chueh,[3] and Ali Javey[1,2,a)]

[1]*Department of Electrical Engineering and Computer Sciences, University of California, Berkeley, California 94720, USA*
[2]*Lawrence Berkeley National Laboratory, Material Sciences Division, Berkeley, California 94720, USA*
[3]*Department of Materials Science and Engineering, National Tsing-Hua University, Hsinchu 30013, Taiwan*
[4]*Lawrence Berkeley National Laboratory, The Molecular Foundry, Berkeley, California 94720, USA*

(Received 5 April 2012; accepted 21 May 2012; published online 25 June 2012)

III–V semiconductor solar cells have demonstrated the highest power conversion efficiencies to date. However, the cost of III-V solar cells has historically been too high to be practical outside of specialty applications. This stems from the cost of raw materials, need for a lattice-matched substrate for single-crystal growth, and complex epitaxial growth processes. To address these challenges, here, we explore the direct non-epitaxial growth of thin poly-crystalline films of III-Vs on metal substrates by using metalorganic chemical vapor deposition. This method minimizes the amount of raw material used while utilizing a low cost substrate. Specifically, we focus on InP which is known to have a low surface recombination velocity of carriers, thereby, making it an ideal candidate for efficient poly-crystalline cells where surface/interface properties at the grain boundaries are critical. The grown InP films are 1-3 μm thick and are composed of micron-sized grains that generally extend from the surface to the Mo substrate. They exhibit similar photoluminescence peak widths and positions as single-crystalline InP, as well as excellent crystallinity as examined through TEM and XRD analyses. This work presents poly-InP as a promising absorber layer for future photovoltaics. © *2012 American Institute of Physics*. [http://dx.doi.org/10.1063/1.4730442]

I. INTRODUCTION

III–V semiconductor solar cells have demonstrated the highest power conversion efficiencies to date.[1] Specifically, InP and GaAs have the most ideal band gaps and highest theoretical efficiencies for single-junction cells. However, the cost of III–V solar cells has historically been too high to be practical outside of specialty applications. This stems from the cost of raw materials, need for a lattice-matched substrate for epitaxial growth of single crystals, and complex epitaxial growth processes.[2,3] To address these issues layer transfer techniques have been explored in the past, where thin epitaxial films of GaAs and InP are selectively peeled and transferred from the growth substrate to a user-defined receiver substrate.[3–8] This process enables the growth substrate to be used multiple times, thereby potentially lowering the manufacturing cost. Here, we explore a different approach, directly growing thin ($\sim$1–3 μm) layers of III–Vs on metal substrates, both thin films and foils. This method minimizes the amount of raw material used and swaps the high-cost substrate for a low-cost one. In addition, metal foils lend themselves to low-cost roll-to-roll processing schemes, act as excellent diffusion barriers to the environment, and exhibit high thermal stability.

Thin film growth on non-epitaxial substrates invariably results in polycrystalline (poly) materials which presents certain constraints and challenges. In particular, the increased surface/interface area and grain boundaries may act as efficient recombination centers for photogenerated minority carriers. Thus, the use of materials with a low surface recombination velocity (SRV) is required to ensure high efficiency poly III–V solar cells. Untreated InP has a drastically lower SRV ($\sim 10^3$ cm s^{-1})[9–15] as compared to GaAs ($\sim 10^6$ cm s^{-1}),[15,16] making it an ideal candidate for efficient poly-crystalline cells. However, while poly-GaAs has been widely explored in the past,[17,18] there have been few reports of poly-InP in terms of growth techniques,[19–21] material quality,[9,22] or device performance.[23,24]

Here, we report on high optical quality poly-InP thin films grown on molybdenum thin film and foil substrates, by metalorganic chemical vapor deposition (MOCVD). The materials and optical characteristics of the grown films are systematically explored as a function of growth conditions. Poly-InP films grown at the optimal temperature exhibit highly promising properties with the photoluminescence spectra closely matching that of a single-crystalline InP. Crystal quality was evaluated as the absence of defects and dislocations, as well as grain size and XRD line width. This work could potentially enable the development of low-cost and yet efficient III-V cells in the future.

II. EXPERIMENTAL DETAILS

A. MOCVD growth

The MOCVD system used was a Thomas Swann 3 × 2 CCS MOCVD. The chamber was a vertical cold-wall

a)Electronic mail: ajavey@berkeley.edu.

showerhead configuration. The susceptor held 3 in. wafers and the rotation rate was fixed at 30 rpm. The precursors were trimethylindium (TMIn) from Akzo Nobel and tert-butylphosphine (TBP) from Dockweiler Chemicals. They were held at 20 °C and 10 °C, respectively. TMIn was flowed at $\sim 1.2 \times 10^{-5}$ mol/min and TBP at $\sim 2.4 \times 10^{-3}$ mol/min, giving a [V]/[III] molar ratio of ~200. Total flow of H_2 and precursors was 11.5 L/min. Growth temperatures ranged from 445 °C to 545 °C. Growth times explored were 5–75 min, with 75 min used for the data in this paper. The chamber pressure was fixed at 76 Torr.

B. Characterization

SEM images were taken on a Zeiss Gemini Ultra-55. TEM was performed using a JEOL-3000 F. The XRD was taken on a Bruker AXS D8 Discover GADDS XRD Diffractometer system. The PL excitation source was a 785 nm laser with ~30 μm spot size, and the detector was a silicon CCD. Note that at this excitation, the penetration depth is ~290 nm, so carriers are being generated mainly in the top quarter of the films. The reference InP sample was (100) orientation n-type doped with zinc to $\sim 10^{17}/cm^3$. The excitation source for the backscatter Raman data was the 488 nm line from an Ar ion laser. The uncertainty of the Raman data is limited to $\pm 0.3\ cm^{-1}$.

III. RESULTS AND DISCUSSION

A. Choice of substrate

The choice of substrate metal is critical for obtaining high quality poly-InP films. At the growth temperature, it should have low solubility of both indium and phosphorus. Ideally, it should either not form indium alloys or metal phosphides or if it does, the reaction should be self-limiting. In addition, it should have a similar thermal expansion coefficient as InP.[24] From metal-P and metal-In phase diagrams, Mo and W meet the above criteria the best. For Mo, in particular, there are no intermetallics at the growth temperature, and the solubility of In is very low. There are few Mo-P compounds, and no solid solutions; this suggests the loss of phosphorous into the substrate will be minimal. Here, we have chosen to focus on Mo, both in the form of thin foils and thin films. The Mo foils used were 25 μm thick and cleaned with acetone and isopropanol prior to growth. In parallel, Si/SiO_2 (thermal oxide, 50 nm thickness) handling wafers with a sputtered Cr (5 nm thickness) adhesion layer and Mo (50 nm thickness) top film were explored as a growth substrate. Subsequently, InP thin films were grown on top of these Mo substrates by MOCVD as schematically illustrated in Figure 1(a). Optical images of InP thin films (~2 μm thickness) grown on flexible Mo foil and sputtered Mo thin film substrates (510 °C and 75 min) are shown in Figures 1(b) and 1(c), respectively. Thus far, we have grown uniform films over ~40 cm^2 foils and 3 in. diameter wafers, limited only by the sample holder size of the MOCVD equipment used in this study. As evident from visual inspection, the grown InP films exhibit large area uniformity and continuity. In general, the growth properties were found to be similar between the two types of substrates. Thus, from here on we primarily present the growth data on the Mo thin film substrate.

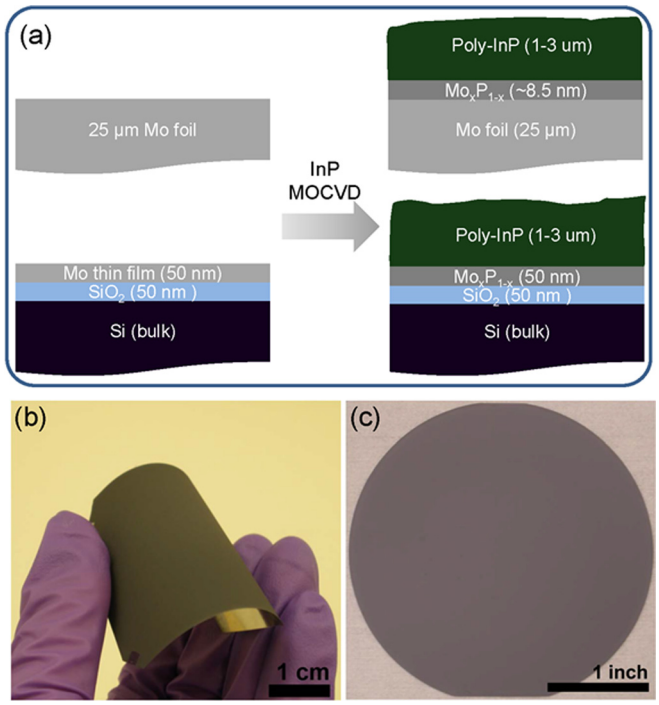

FIG. 1. (a) Poly-InP fabrication scheme; (b) poly-InP on flexible molybdenum foil; (c) poly-InP on sputtered Mo on 3 in. wafer. Lighter ring is due to edge effects from the susceptor.

B. SEM/TEM

In this work, we primarily focus on the effects of growth time and temperature. Figures 2(a) and 2(b) show top-and side-view SEM images of a representative InP thin film (~3 μm thickness) grown on a Mo thin film. The growth temperature and time were 520 °C and 75 min, respectively, which were optimal given the opposing constraints of surface coverage and crystal quality. The grown InP films are poly-crystalline and continuous (Figures 2(a) and 2(b)). The grains generally extend from the surface to the substrate but are oriented randomly. The average grain size and surface roughness of the thin film for this growth condition are ~2 μm and ~200 nm, respectively—both of which highly depend on the growth temperature.

From SEM and TEM analyses, the grain sizes range from ~0.5 μm at 445 °C growth temperature to ~10 μm at 545 °C (Figure 3). While the grain size increases with temperature, the grown InP is not continuous at ≥545 °C for a fixed growth time of 75 min. Higher substrate temperatures increase the desorption rate of precursors from the substrate, which causes a reduced number of nucleation sites. In addition, the existing nucleation sites grow and deplete the local environment of precursors at the expense of additional nucleation, which results in a discontinuous film. At growth temperatures of ≤500 °C, striations are clearly present within each grain oriented parallel to the substrate based on SEM inspection (Figure 4). From TEM analysis, the striations correspond to stacking faults (Figure 4). Each layer appears to consist of

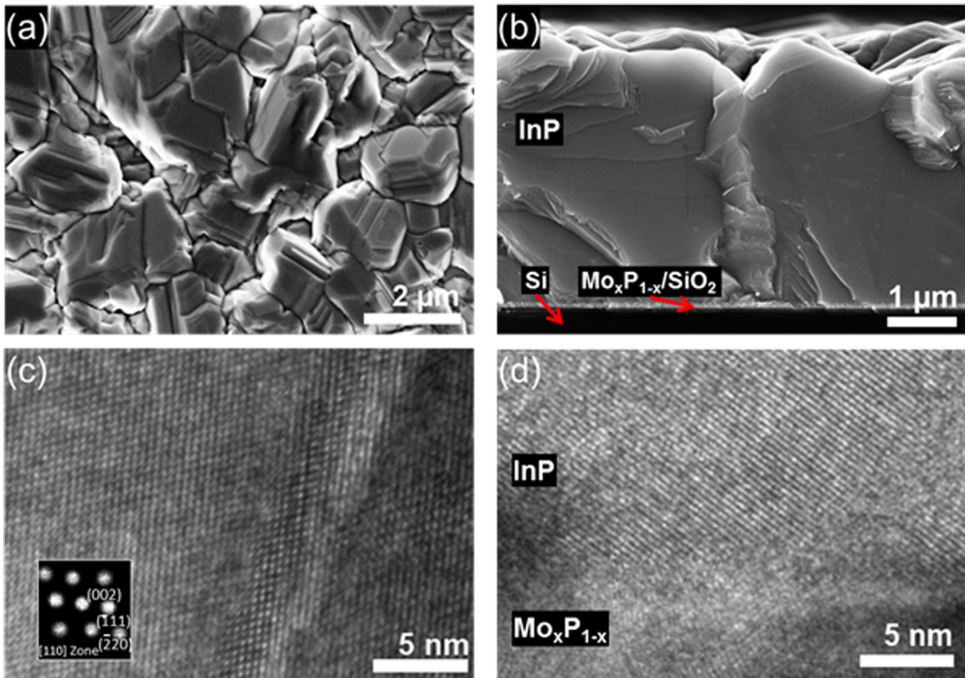

FIG. 2. (a) SEM top view of poly-InP grown at 520 °C for 75 min. (b) Cross-sectional SEM image of poly-InP grown on a Mo thin film at 520 °C for 75 min. The InP is on top of ~50 nm Mo_xP_{1-x}/50 nm SiO_2/Si. (c) TEM image at a grain boundary. Inset shows FFT from within the left grain. (d) TEM of interface between InP and Mo/Mo_xP_{1-x}.

~10–100 close packed planes. Similar stacking faults and twinning have been observed in metalorganic vapor phase epitaxy grown InP nanowires in the [111] direction.[25,26] The data are also consistent with the known low stacking fault energy of InP.[27] However, at growth temperatures of ≥520 °C, the density of stacking faults is drastically reduced with only a minimal number of such defects being evident in TEM analysis (Figure 2(c)). The appearance of stacking faults suggests the growth mechanism after nucleation is layer-by-layer of close packed planes ([111] direction in a zincblende lattice). This is similar to the traditional growth of epitaxial layers, where the underlying substrate is cut slightly off axis to facilitate layer-by-layer growth at terraces. Altogether, crystal quality appears to be higher at higher growth temperatures. Considering both crystal quality and film continuity constraints, 520 °C is found to be the optimal growth temperature for a fixed growth time of 75 min.

Further, TEM study indicates the interface between InP and Mo is continuous and free of voids, as seen in Figure 2(d). Composition analysis reveals significant phosphorus content throughout the initial 50 nm Mo layer. It appears to be composed of a mixture of Mo and Mo_xP_{1-x} phases, where x ranges from ~0.8 to ~0.5 from low to high growth temperatures as confirmed by energy-dispersive X-ray spectroscopy/TEM analysis. In contrast, InP on Mo foil samples showed a similar Mo_xP_{1-x} layer, where x ranged from ~0.6 to ~0.4. However, this layer was self-limited to a thickness of only ~8.5 nm (Figure 5). This is attributed to the larger grain sizes of the foil vs. the sputtered Mo, and corresponding lower reactivity. Close examination reveals that in some locations, the InP lattice matches that of the underlying Mo_xP_{1-x}, suggesting a high quality interface. Note that in contrast to the results here, Ni foil substrates in the same growth conditions showed uncontrollable reactions with phosphorus and indium. This is consistent

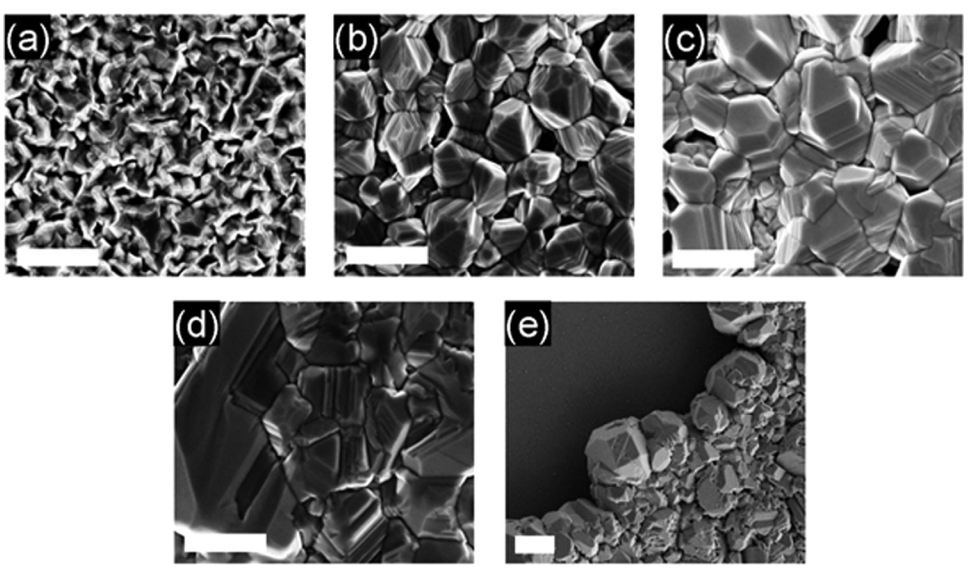

FIG. 3. Growth temperature series showing increasing grain size with growth temperature. Samples shown are all grown on sputtered Mo thin films. (a) 445 °C, (b) 480 °C, (c) 500 °C, (d) 520 °C, and (e) 545 °C. Scale bars in (a)–(d) are 2 μm, scale bar in (e) is 10 μm.

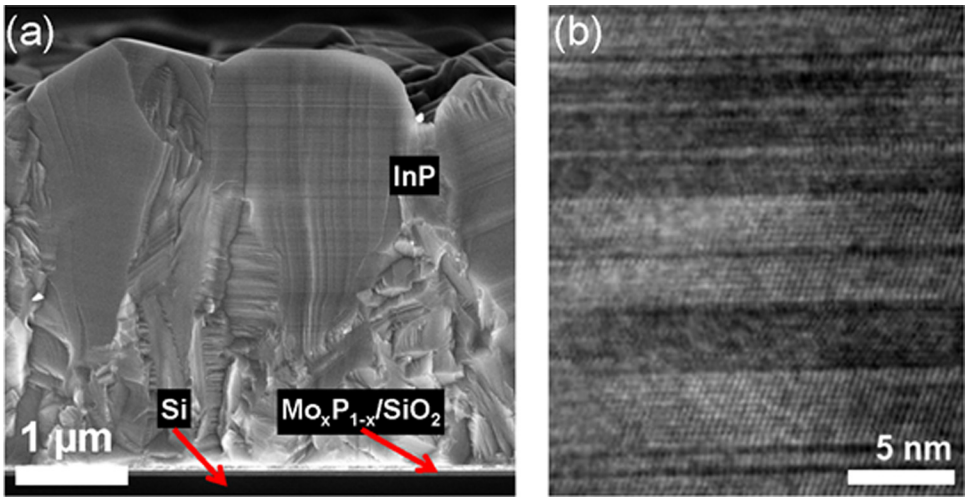

FIG. 4. (a) Side view SEM image of sample grown on a Mo thin film at 500 °C for 75 min. A grain without striations (left) is shown next to two with horizontal striations (right). (b) TEM image of same sample showing stacking faults.

with presence of solid solutions at the growth temperatures in the In-Ni and Ni-P phase diagrams. The surface of the foils becomes pitted and cracked and no InP film was able to grow.

C. XRD

The grown InP films were characterized by XRD (Figure 6). The XRD analysis further shows texture at lower growth temperatures, with only the (111) and (222) peaks noticeable. The peak positions match those of zincblende InP.[28,29] As the growth temperature increases, additional peaks appear, indicating the grains become more randomly oriented. This implies that at lower growth temperatures there is a preferential orientation for nucleation sites, and at higher temperatures there is not. Growth after nucleation naturally follows the orientation of the nuclei. At the highest growth temperature of 545 °C, the relative peak intensities are a close match to the International Centre for Diffraction Data (ICDD) powder reference.[29] In addition, the line widths of the (220) and (311) peaks get progressively narrower as growth temperature increases, indicating a greater level of crystallinity. There is no evidence of wurtzite InP peaks,[28] especially the (0002) peak which would show up close to (111) zincblende peak, indicating that the stacking faults do not result in a phase change from zincblende to wurtzite.

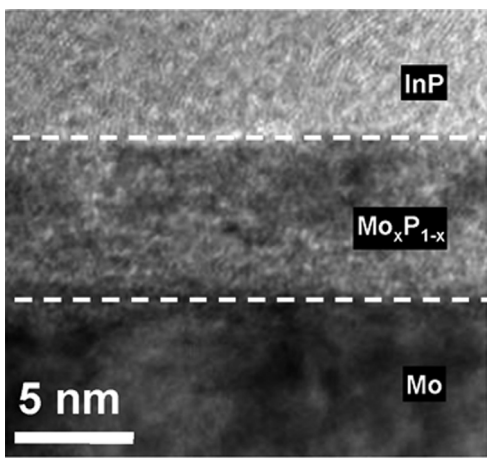

FIG. 5. TEM image of the ~8.5 nm transition layer of Mo_xP_{1-x} between InP (top) and Mo foil (bottom).

D. Raman

Raman spectra (Figure 7) for films grown at all temperatures (445 °C–545 °C) match well with that reported in the literature for a single-crystalline InP substrate.[30–32] The first order anti-Stokes ΓTO and ΓLO peaks show up at ~303 cm^{-1} and ~344 cm^{-1}, respectively. The data are all normalized to the ΓTO peak intensity. The relative intensity of the ΓLO peak increases slightly with growth temperature. In addition, the ΓLO peak shows a pronounced asymmetry towards lower energy. Second order features corresponding to the XLO + XTO, 2ΓTO, and ΓLO + ΓTO interactions also appeared.[30,32] Of these, only the XLO + XTO feature intensity showed a strong correlation with growth temperature, which may be related to the stacking fault density. While the intensity increases with growth temperature, the shape remains unchanged. From the zincblende symmetry selection rules, the LO phonon peak appears if the surface is (100) or (111), while the TO phonon peak appears if the

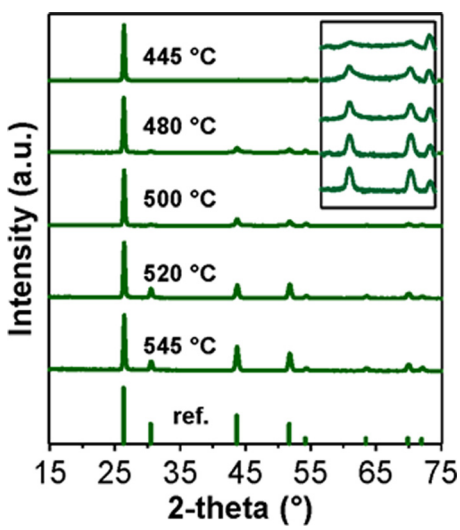

FIG. 6. XRD spectra as a function of growth temperature. Curves are normalized to the (111) peak and offset. Inset, log scale, shows the gradual narrowing of the (220) and (311) peaks. Reference data are from the International Centre for Diffraction Data (ICDD) Powder Diffraction File (PDF). From left to right, the first five peaks are as follows: (111), (200), (220), (311), and (222).

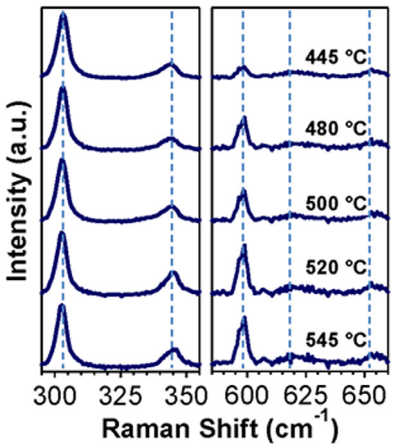

FIG. 7. Room temperature Raman. Data are normalized to the ΓTO peak and offset. The left graph shows the first order peaks, ΓTO and ΓLO, from left to right. The right graph shows second order peaks, XLO + XTO, 2ΓTO, and ΓLO + ΓTO, from left to right. Intensity of data in right graph is 5×.

surface is (110) or (111). The presence of both peaks is consistent with the (111) texture seen at lower growth temperatures and the randomly oriented grains at higher growth temperatures. There are no indications of stress in the films as indicated by peak positions.

E. Photoluminescence

Room temperature micro-PL data also show a clear trend of increasing quality with growth temperature (Figure 8). As a metric, we compare our poly-InP PL spectra to a non-degenerately doped single crystal InP reference, as well as previously reported values in the literature. At the two highest growth temperatures (520 °C and 545 °C), the peak position, full-width-at-half-maximum (FWHM), and shape are nearly identical to a single-crystal reference sample. Although the level of unintentional doping is unknown, this is evidence that the optical qualities of poly-InP are comparable to single crystal InP. At lower growth temperatures, the spectra are blue-shifted, FWHM is broad, and the shape is symmetric. The trend is summarized in Table I. Note that the 520 °C and 545 °C peaks at ∼922 nm correspond to the direct band gap energy of ∼1.34 eV,[33,34] matching closely the

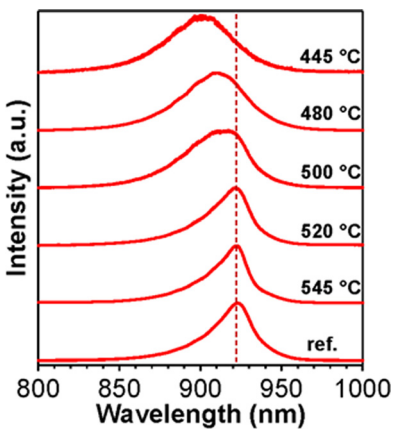

FIG. 8. Room temperature PL changes with growth temperature. Higher growth temperatures exhibit near identical shape and position as a single crystal reference. Curves are normalized and offset.

TABLE I. PL peak positions and FWHMs as a function of growth temperature.

Growth temperature (°C)	Peak position (nm)	FWHM (nm)
445	898.5	46
480	908.8	46
500	917.0	45
520	921.6	30
545	922.4	26
Ref. single crystal sample	923.4	28

expected band-gap of InP, whereas the 445 °C peak at ∼898.5 nm corresponds to ∼1.38 eV. Such blue-shifts have been observed for InP nanowires with stacking faults and have been attributed to the presence of the wurtzite phase or quantum confinement, both of which increase the band gap.[25,35] While there is clearly a correlation between stacking fault prevalence due to growth temperature and PL characteristics in our InP, the SEM, and XRD data do not indicate the presence of a wurtzite phase.

Also, important to note is that the PL feature from the 500 °C sample is plainly composed of two overlapping peaks, as can be seen by the asymmetry and flat top. Moreover, the relative intensities of the two contributions varied as the sample was scanned laterally (not shown). This is consistent with the SEM/TEM analyses, which shows grains with stacking faults next to those without such defects. There is also a clear transition temperature between 500 °C and 520 °C where the optical transitions corresponding to the higher energy peak are totally suppressed, leaving only the peak corresponding to bulk zincblende InP. This possibly corresponds to the elimination of stacking faults. There is a strong correlation between the presence of stacking faults and the higher energy PL feature. However, without conclusive evidence and a satisfactory model for this hypothesis, we cannot establish a causal relationship. The possibility of other defects introduced at low growth temperatures cannot be ruled out as the source of the PL trend. Based on the PL characteristics, the optimal growth temperature is at 520 °C. At this growth temperature, there are no PL features remaining that do not appear in the single crystal reference.

IV. CONCLUSIONS

To summarize, we have demonstrated high optical quality InP grown on metal substrates. The resulting films are composed of micron-sized grains and importantly show nearly identical PL and Raman spectral shape and position as those of a single-crystal reference. In the future, further characterization of the minority carrier lifetime, mobility, and diffusion length is needed. Doping and the particulars of full device fabrication need to be worked out as well. Our growth scheme avoids using expensive single-crystal substrates and associated complex epitaxial structures, which have thus far hindered the market success of III–V solar cells. Metal foil substrates not only reduce cost at the material growth step but also at downstream processing steps. For example, flexible foil substrates are a natural fit for roll-to-

roll processing.[36] They are robust, light-weight, and act as excellent barriers to the environment. Poly-InP grown using our technique shows great promise for high-efficiency, low-cost solar cells.

ACKNOWLEDGMENTS

This work was supported by the Director, Office of Science, Office of Basic Energy Sciences, Materials Sciences, and Engineering Division of the U.S. Department of Energy under Contract No. DE-AC02-05CH11231. A.J. acknowledges support from the World Class University program at Sunchon National University.

[1]M. A. Green, K. Emery, Y. Hishikawa, and W. Warta, Prog. Photovoltaics **19**, 84 (2011).
[2]C. J. Keavney, V. E. Haven, and S. M. Vernon, in *Conference Record of the 21st IEEE Photovoltaic Specialists Conference* (1990), Vol. 1, p. 141.
[3]M. W. Wanlass, T. J. Coutts, J. S. Ward, and K. A. Emery, in *Conference Record of the 22nd IEEE Photovoltaic Specialists Conference* (1991), Vol. 1, p. 159.
[4]J. Yoon, S. Jo, I. S. Chun, I. Jung, H.-S. Kim, M. Meitl, E. Menard, X. Li, J. J. Coleman, U. Paik, and J. A. Rogers, Nature **465**, 329 (2010).
[5]X. Y. Lee, A. K. Verma, C. Q. Wu, M. Goertemiller, E. Yablonovitch, J. Eldredge, and D. Lillington, in *Conference Record of the 25th IEEE Photovoltaic Specialists Conference* (1996), p. 53.
[6]J. M. Zahler, K. Tanabe, C. Ladous, T. Pinnington, F. D. Newman, and H. A. Atwater, Appl. Phys. Lett. **91**, 012108 (2007).
[7]J. M. Zahler, A. Fontcuberta i Morral, C.-G. Ahn, H. A. Atwater, M. W. Wanlass, C. Chu, and P. A. Iles, in *Conference Record of the 29th IEEE Photovoltaic Specialists Conference* (2002), p. 1039.
[8]K. Lee, K.-T. Shiu, J. D. Zimmerman, C. K. Renshaw, and S. R. Forrest, Appl. Phys. Lett. **97**, 101107 (2010).
[9]T. Nakamura and T. Katoda, J. Appl. Phys. **55**, 3064 (1984).
[10]Y. Rosenwaks, Y. Shapira, and D. Huppert, Phys. Rev. B **44**, 13097 (1991).
[11]R. K. Ahrenkiel, D. J. Dunlavy, and T. Hanak, J. Appl. Phys. **64**, 1916 (1988).
[12]R. K. Ahrenkiel, D. J. Dunlavy, and T. Hanak, Sol. Cells **24**, 339 (1988).
[13]Y. Rosenwaks, Y. Shapira, and D. Huppert, Phys. Rev. B **45**, 9108 (1992).
[14]S. Bothra, S. Tyagi, S. K. Ghandhi, and J. M. Borrego, Solid-State Electron. **34**, 47 (1991).
[15]D. D. Nolte, Solid-State Electron. **33**, 295 (1990).
[16]L. Jastrzebski, J. Lagowski, and H. C. Gatos, Appl. Phys. Lett. **27**, 537 (1975).
[17]R. Venkatasubramanian, B. C. O'Quinn, J. S. Hills, P. R. Sharps, M. L. Timmons, J. A. Hutchby, H. Field, R. Ahrenkiel, and B. Keyes, in *Conference Record of the 25th IEEE Photovoltaic Specialists Conference* (1996), p. 31.
[18]Y. C. M. Yeh and R. J. Stirn, Appl. Phys. Lett. **33**, 401 (1978).
[19]T. Saitoh, S. Matsubara, and S. Minagawa, Thin Solid Films **48**, 339 (1978).
[20]T. Saitoh, S. Matsubara, and S. Minagawa, Jpn. J. Appl. Phys., Part 1 **15**, 893 (1976).
[21]T. Saitoh, S. Matsubara, and S. Minagawa, J. Electrochem. Soc. **123**, 403 (1976).
[22]T. Saitoh and S. Matsubara, J. Electrochem. Soc. **124**, 1065 (1977).
[23]T. Saitoh, S. Matsubara, and S. Minagawa, Jpn. J. Appl. Phys., Part 1 **16**, 807 (1977).
[24]K. J. Bachmann, E. Buehler, J. L. Shay, and S. Wagner, Appl. Phys. Lett. **29**, 121 (1976).
[25]R. L. Woo, R. Xiao, Y. Kobayashi, L. Gao, N. Goel, M. K. Hudait, T. E. Mallouk, and R. F. Hicks, Nano Lett. **8**, 4664 (2008).
[26]R. E. Algra, M. A. Verheijen, M. T. Borgstrom, L.-F. Feiner, G. Immink, W. J. P. van Enckevort, E. Vlieg, and E. P. A. M. Bakkers, Nature **456**, 369 (2008).
[27]H. Gottschalk, G. Patzer, and H. Alexander, Phys. Status Solidi A **45**, 207 (1978).
[28]P. I. Gaiduk, F. F. Komarov, V. S. Tishkov, W. Wesch, and E. Wendler, Phys. Rev. B **61**, 15785 (2000).
[29]ICDD PDF-2, Entry 00-032-0452, 2003.
[30]G. F. Alfrey and P. H. Borcherds, J. Phys. C **5**, L275 (1972).
[31]A. Mooradian and G. B. Wright, Solid State Commun. **4**, 431 (1966).
[32]L. Artús, R. Cuscó, J. M. Martín, and G. González-Díaz, Phys. Rev. B **50**, 11552 (1994).
[33]W. J. Turner, W. E. Reese, and G. D. Pettit, Phys. Rev. **136**, A1467 (1964).
[34]M. Bugajski and W. Lewandowski, J. Appl. Phys. **57**, 521 (1985).
[35]G. Perna, V. Capozzi, V. Augelli, T. Ligonzo, L. Schiavulli, G. Bruno, M. Losurdo, P. Capezzuto, J. L. Staehli, and M. Pallara, Semicond. Sci. Technol. **16**, 377 (2001).
[36]M. H. Lee, N. Lim, D. J. Ruebusch, A. Jamshidi, R. Kapadia, R. Lee, T. J. Seok, K. Takei, K. Y. Cho, Z. Fan, H. Jang, M. Wu, G. Cho, and A. Javey, Nano Lett. **11**, 3425 (2011).